Original Article
Yonsei Med J 2020 Sep;61(9):816-825
https://doi.org/10.3349/ymj.2020.61.9.816
Yonsei Medical Journal
YMJ
pISSN: 0513-5796 · eISSN: 1976-2437

Induced Pluripotent Stem Cell Modeling of Best Disease and Autosomal Recessive Bestrophinopathy

Ji Hwan Lee, Jin-ok Oh, and Christopher Seungkyu Lee

Department of Ophthalmology, The Institute of Vision Research, Yonsei University College of Medicine, Seoul, Korea.

Purpose: To understand the pathophysiology of Best disease (BD) and autosomal recessive bestrophinopathy (ARB) by establishing an in vitro model using human induced pluripotent stem cell (iPSC).

Materials and Methods: Human iPSC lines were generated from mononuclear cells in peripheral blood of one ARB patient, one autosomal dominant BD patient, and two normal controls. Immunocytochemistry and reverse transcriptase polymerase chain reaction in iPSC lines were conducted to demonstrate the pluripotent markers. After the differentiation of iPSC into functional retinal pigment epithelium (RPE), morphological characteristics of the RPE were evaluated using confocal microscopy and immunocytochemistry. The rates of fluid flow across iPSC-RPE monolayer were measured to compare apical to basal fluid transports by RPE. RNA sequencing was performed on iPSC-RPE to identify the differences in gene expression profiles, and specific gene sets were tested using Gene Set Enrichment Analysis.

Results: Morphological characteristics, gene expression, and epithelial integrity of ARB iPSC were comparable to those of BD patient or normal control. Fluid transport from apical to basal was significantly decreased in ARB iPSC-RPE compared with BD iPSC-RPE or control iPSC-RPE. Gene Set Enrichment Analysis confirmed that ARB iPSC-RPE exhibited significant enrichments of epithelial-mesenchymal transition gene set and TNF-α signaling via NF-κB gene set compared to control iPSC-RPE or BD iPSC-RPE.

Conclusion: A human iPSC model of ARB showed a functional deficiency rather than anatomical defects. ARB may be caused by RPE dysfunction following *BEST1* mutation.

Key Words: Induced pluripotent stem cells, retinal pigment epithelium, vitelliform macular dystrophy

INTRODUCTION

Hereditary retinal disease is one of the important causes of blindness, which leads to an irreversible retinal damage affecting the quality of life and daily activities. Bestrophinopathy is one of the most common inherited macular degenerations, and it is caused by mutations in the *BEST1* gene. *BEST1* is located in chromosome 11q13,[1,2] and encodes a 585 amino acid protein known as bestrophin that localizes to the basolateral membrane of the retinal pigment epithelium (RPE).[3] When mutated, lipofuscin accumulates beneath the RPE, with degeneration of the RPE and the overlying photoreceptors.[4] The broad spectrum of clinical presentations in bestrophinopathy ranges from well-defined clinical abnormalities restricted to the macula in Best disease [BD, also known as vitelliform macular dystrophy; Online Mendelian Inheritance in Man (OMIM) 153700] and autosomal recessive bestrophinopathy (ARB; OMIM 611809) to the widespread symptoms affecting peripheral retina in a rare condition of autosomal dominant vitreoretinochoroidopathy (ADVIRC; OMIM 193220).[5,6]

BD was first described by Friedrich Best in 1905,[7] and is most common among bestrophinopathies. BD occurs in about 1 in every 10000 individuals, and is inherited by autosomal dominant fashion.[6] The age at onset of BD is variable, with a mean age onset in the fourth decade.[8] The macular lesion that is most characteristic of the disease is single egg-yolk-like vitelliform lesion on the central fovea, which is usually followed by vitel-

Received: June 2, 2020 **Revised:** July 17, 2020
Accepted: August 11, 2020
Corresponding author: Christopher Seungkyu Lee, MD, PhD, Department of Ophthalmology, Yonsei University College of Medicine, 50-1 Yonsei-ro, Seodaemun-gu, Seoul 03722, Korea.
Tel: 82-2-2228-3576, Fax: 82-2-312-0541, E-mail: sklee219@yuhs.ac

•The authors have no potential conflicts of interest to disclose.

liruptive stage, pseudohypopyon stage, and atrophic stage.[6] A significantly decreased light rise on electrooculography (EOG) is a characteristic finding of BD.[9] Although an abnormal EOG is crucial in the diagnosis of BD in patients with vitelliform lesions, mutation analysis is necessary to confirm a clinical diagnosis of BD since 20% of patients with *BEST1* mutation could have a normal EOG.[10]

BEST1 mutation has long been believed to segregate only in an autosomal dominant manner. Then, autosomal recessive disease with *BEST1* mutation was first defined as a distinct category of bestrophinopathy by Burgess, et al.[11] in 2008, which is now widely known as ARB.[6] Nearly 40 biallelic mutations in *BEST1* have been reported in ARB patients to date.[12-15] Retinopathy includes an irregularity of the RPE throughout the posterior fundus with punctate flecks, which is easily seen on autofluorescence imaging. Retinal edema and subretinal fluid are common findings on OCT imaging. ARB shows markedly abnormal EOG and pattern electroretinography (ERG).[11]

Human induced pluripotent stem cells (iPSC) are relatively non-invasive and renewable, and iPSC-derived models can recapitulate cellular and molecular processes without genetic manipulation.[16] The retina and the brain are promising candidates for iPSC modeling as it is difficult to perform biopsy in these tissues, and there are established preexisting protocols to isolate their progenitors from iPSC.[17-19] The RPE can be readily differentiated and re-seeded widely, which is a promising candidate for iPSC modeling. In this study, we sought to model BD and ARB using iPSC technology, which would be useful in studying the pathophysiology and therapeutic targets of *BEST1*-associated retinopathy.

MATERIALS AND METHODS

Differentiation of human iPSC lines

Generation of iPSC lines

This study was approved by the Institutional Review Board of Severance Hospital, Yonsei University College of Medicine (3-2017-0167). Twenty milliliters of peripheral blood were obtained from one ARB patient (L40P and A195V mutations in *BEST1* gene), one autosomal dominant BD patient (G96A mutation in BEST1 gene), and two normal controls. Human iPSC lines were generated using previously established methods.[17,18] Mononuclear cells (MNC) were isolated from the blood samples and were expanded in MNC media for 7–10 days.

MNC were transfected with episomal vectors (OCT4, SOX2, c-MYC, KLF4, LIN28) (Thermo Fisher Scientific, Waltham, MA, USA) and cultured on extracellular matrices (BD, Franklin Lakes, NJ, USA). Culture on iPSC medium (STEMCELL Technologies, Vancouver, Canada) were performed for 1–2 weeks till colonization of iPSC. iPSC colonies were isolated and expanded on iPSC medium (STEMCELL Technologies). Differentiation was initiated after 10–20 passages of expansion to remove an epigenetic memory.

Differentiation of iPSC into functional RPE cell

Embryoid body (EB) was formed for 1 week on EB media (Thermo Fisher Scientific) and free-floating culture. EB was then switched to a chemically defined neural induction media (Thermo Fisher Scientific) and laminin-coated plate (Thermo Fisher Scientific) for 10 days for neural differentiation. For retinal differentiation, iPSC-derived neuroepithelial rosettes were switched to a chemically defined retinal differentiation medium (Thermo Fisher Scientific).

RT-PCR

Total RNA was isolated from cell cultures from various stages of differentiation and treated with DNase I (Thermo Fisher Scientific). cDNA was synthesized using the SuperScript III RT-PCR kit (Thermo Fisher Scientific). Samples were denatured at 95°C for 5 minutes followed by 30 cycles of PCR amplification (95°C for 15 seconds, 60°C for 30 seconds, 72°C for 1 minute) and a final extension at 72°C for 10 minutes. PCR products were run on 2% agarose gel.

Immunocytochemistry

Cells were washed in ice-cold phosphate-buffered saline (PBS) and fixed in 2–4% paraformaldehyde at 4°C for 30 minutes. Fixed cells were washed twice in PBS and placed in blocking solution (10% normal donkey or goat serum and 0.01–0.05% Triton-X100 in PBS) for 1 hour at room temperature. Cells were then incubated overnight at 4°C with mouse anti-*BEST1* monoclonal antibody (E6-6) (Thermo Fisher Scientific) and rabbit anti-ZO-1 polyclonal antibody (Thermo Fisher Scientific). The following day, cells were washed three to five times in PBS with 0.01% Triton-X100 and incubated with Alexa Fluor 488-conjugated goat anti-rabbit antibody (Thermo Fisher Scientific) and Alexa Fluor 568-conjugated donkey anti-rabbit antibody (Thermo Fisher Scientific). After secondary antibody incubation, cells were stained with DAPI (Thermo Fisher Scientific), washed three times in PBS with 0.2% Triton-X100, and imaged on a confocal microscope (Zeiss, Jena, Germany).

Transepithelial resistance (TER) measurement

TER of RPE monolayers cultured on permeable transwell filters (Merck KGaA, Darmstadt, Germany) was measured using an epithelial voltohmmeter (Merck KGaA) according to manufacturer's instructions. Electrodes were sterilized with 70% ethanol and rinsed in Hank's balanced salt solution prior to placement in the transwell inserts. Net TER was calculated by subtracting the background measurement obtained from transwell filters and multiplying the difference by the area of the transwell filter (Ω^*cm^2).

Table 1. Demographics and Characteristics of Patients and Normal Controls

Patient	Sex	Age	Diagnosis	ERG	EOG	Inheritance	*BEST1* mutation	Amino acid change
NL 1	F	46	NL control	NL	NL	NA	NA	NA
NL 2	M	44	NL control	NL	NL	NA	NA	NA
Patient 1	F	41	BD	NL	Flat	AD	c.287A>G	Gln96Arg
Patient 2	F	57	ARB	NL	Flat	AR	c.119T>C c.584C>T	Leu40Pro Ala195Val

AD, autosomal dominant; AR, autosomal recessive; ARB, autosomal recessive bestrophinopathy; BD, Best disease; EOG, electrooculography; ERG, electroretinography; NA, not applicable; NL, normal; F, female; M, male.

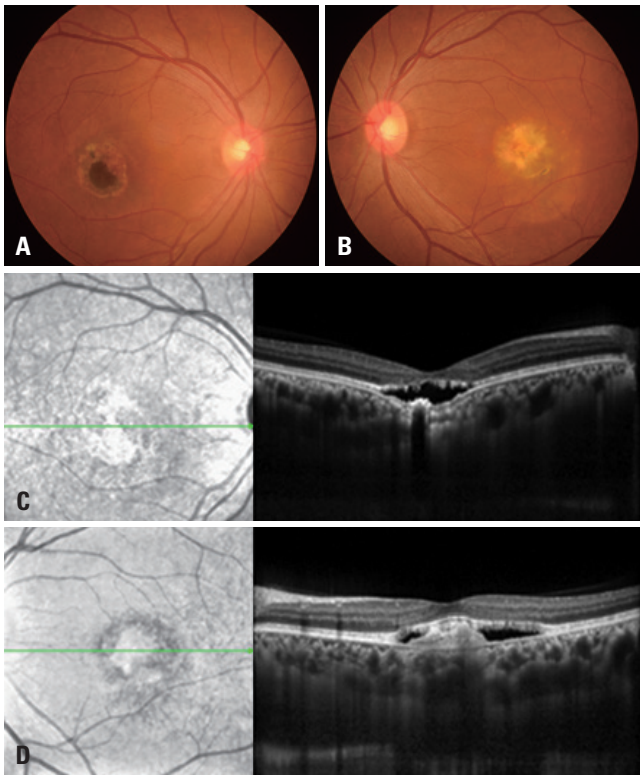

Fig. 1. Clinical findings of Patient 1. A 41-year-old woman presented with decreased visual acuity in the right eye. (A and B) Color fundus photography showed RPE atrophy and pigment disruption in the right eye and a dome-shaped accumulation of yellowish material in the central macula of the left eye. (C and D) Hyperreflective materials with subretinal fluid were found in the subretinal space on optical coherence tomographic images. RPE, retinal pigment epithelium.

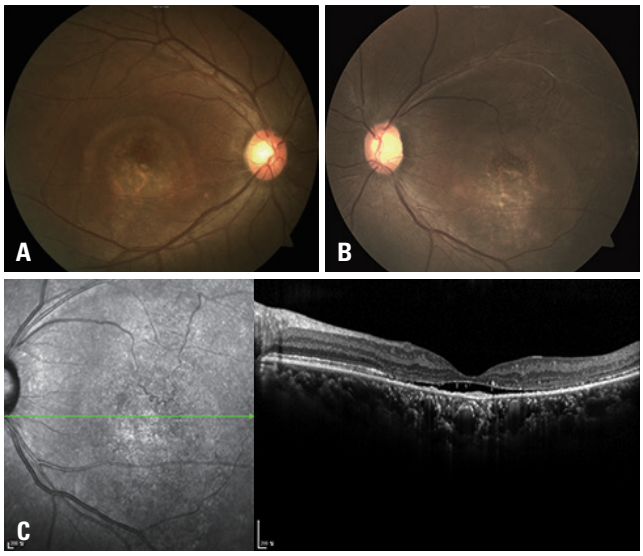

Fig. 2. Clinical findings of Patient 2. A-57-year-old woman presented with decreased visual acuity in her left eye for 2 months. She had reported significant visual loss in both eyes at the age of 20 years. (A and B) Color fundus photography showed bilateral RPE irregularities in the posterior pole with scattered yellowish flecks. (C) A neurosensory retinal detachment with subretinal fluid was observed in the left eye on an optical coherence tomography image, which appeared similar to that of the fellow eye. RPE, retinal pigment epithelium.

Measurement of fluid flux

The quantification of active fluid transport from apical to basal side in the RPE was measured using a previously described method.[20] A fixed amount of medium (Thermo Fisher Scientific), 150 μL in the apical and 400 μL in the basal chambers of transwell, was loaded. The amount of fluid remaining in the apical chamber was measured 20 hours later, and the rate of fluid transport was calculated (μL/hr/cm^2).

RNA sequencing and data analysis

RNA sequencing was performed on ARB iPSC-RPE, BD iPSC-RPE, and normal iPSC-RPE (n=2 for each) using the Macrogen (Seoul, Korea). Total RNA quality was assessed with Agilent bioanalyzer system (Agilent, Santa Clara, CA, USA). Extracted RNA samples were processed with TruSeq Stranded Total RNA Prep Kit (Illumina, San Diego, CA, USA) and sequenced on NovaSeq 6000 system (Illumina). A median 1.2×10^8 single-end reads (range, 1.1×10^8 to 1.3×10^8) with 101 base pairs were generated. Reads were trimmed based on sequencing quality using Trimmomatic (RWTH Aachen University, Aachen, Germany).[21] Trimmed reads were aligned on a human reference sequence (hg19) using HISAT2 (Johns Hopkins University, Baltimore, MD, USA).[22] Using Gene Set Enrichment Analysis, an enrichment of a specific gene set was tested, and core enrichment genes were determined.[23]

Statistical analysis

All statistical analyses were performed using SPSS version 23.0 (IBM Corp., Armonk, NY, USA). Shapiro-Wilk test was used to assess distribution patterns of data. TER measurement and the

https://doi.org/10.3349/ymj.2020.61.9.816

rate of fluid flow obtained from ARB iPSC-RPE were compared with those of control and BD iPSC-RPE using Mann-Whitney test. A p-value <0.05 was considered statistically significant.

RESULTS

Clinical findings

Demographics and characteristics of patient with Best vitelliform macular dystrophy and patient with ARB are summarized in Table 1. Patient 1 was a 41-year-old woman with decreased visual acuity in the right eye. Her best-corrected visual acuity was 20/40 in the right eye and 20/20 in the left eye. The patient was hyperopic with spherical equivalent +1.75 diopter (OD) and +1.00 diopter (OS). The fundus showed RPE atrophy and pigment disruption in the right eye and a dome-shaped accumulation of yellowish material in the central macula of the left eye (Fig. 1A and B). Hyperreflective vitelliform materials with sub-

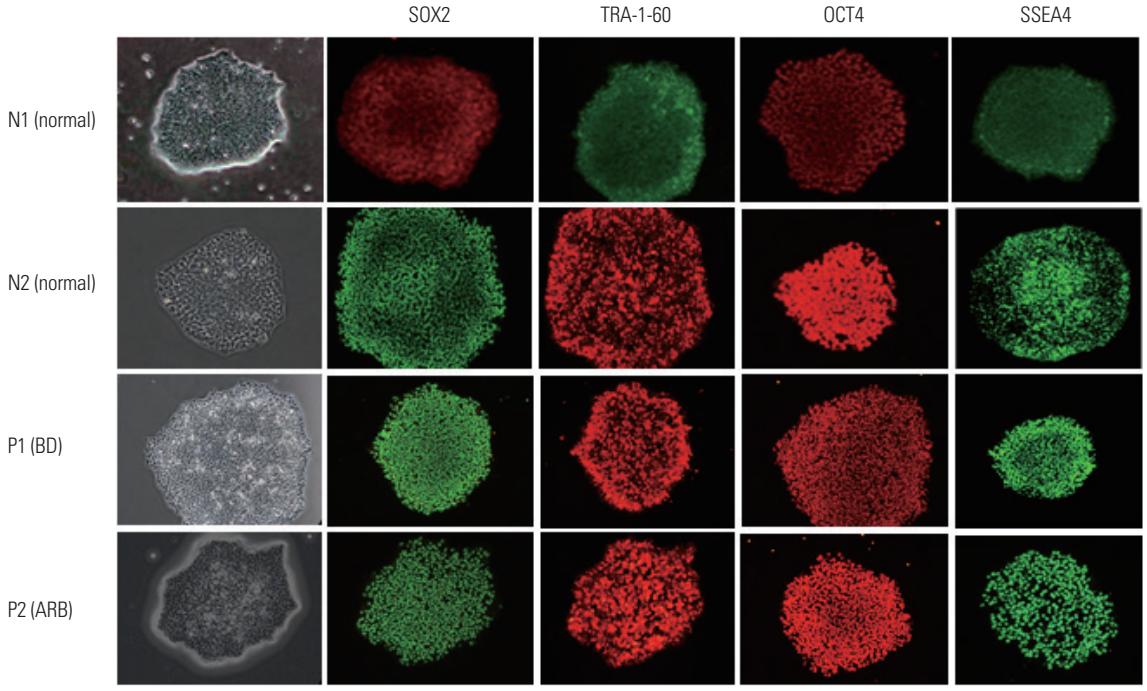

Fig. 3. Immunocytochemistry in iPSC lines. Immunocytochemistry analysis demonstrated the expression of pluripotency markers (OCT4, SOX2, TRA1-60, and SSEA4) in all iPSC lines of normal controls and patients. iPSC, induced pluripotent stem cell; BD, Best disease; ARB, autosomal recessive bestrophinopathy.

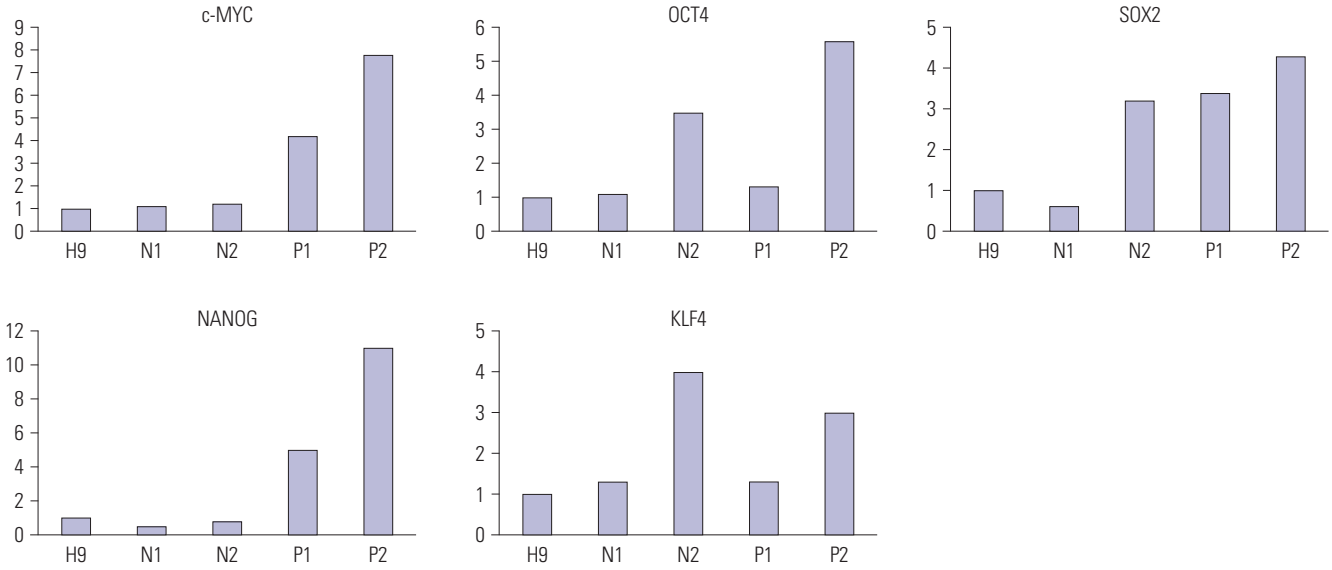

Fig. 4. RT-PCR in iPSC lines. RT-PCR revealed mRNA expression of pluripotency markers (c-MYC, OCT4, SOX2, NANOG, and KLF4) in undifferentiated iPSC lines from normal controls and patients. Human embryonic stem cells (H9) were used as a positive control. iPSC, induced pluripotent stem cell.

retinal fluid were found in the subretinal space on OCT images (Fig. 1C and D). EOG showed decreased response with Arden ratio 1.1 in both eyes.

Patient 2 was a 57-year-old woman who reported significant visual loss in both eyes at the age of 20 years. She presented with a further decrease of the visual acuity in her left eye for 2 months. Her visual acuity was 20/400 in the right eye and 20/800 in the left eye. The patient was hyperopic with spherical equivalent +3.00 diopter (OD) and +3.25 diopter (OS). The fundus showed bilateral RPE irregularities in the posterior pole with scattered yellowish flecks (Fig. 2A and B), which were more prominent on autofluorescence images. A neurosensory retinal detachment with subretinal fluid was observed in the left eye on an OCT image, which appeared similar to that of the fellow eye (Fig. 2C). Electrophysiology showed normal response for the full-field ERG, but a light rise on EOG was absent (Arden ratio 1.0) in both eyes.

Generation of iPSC lines

MNC were isolated from peripheral blood, and iPSC lines were generated using previously established methods.[17,18] Immunocytochemistry and RT-PCR in iPSC lines were performed to confirm the pluripotent markers. Immunocytochemistry analysis using confocal microscopy demonstrated that all iPSC lines expressed the pluripotent markers including OCT4, SOX2, TRA-1-60, and SSEA4 (Fig. 3). RT-PCR revealed pluripotency

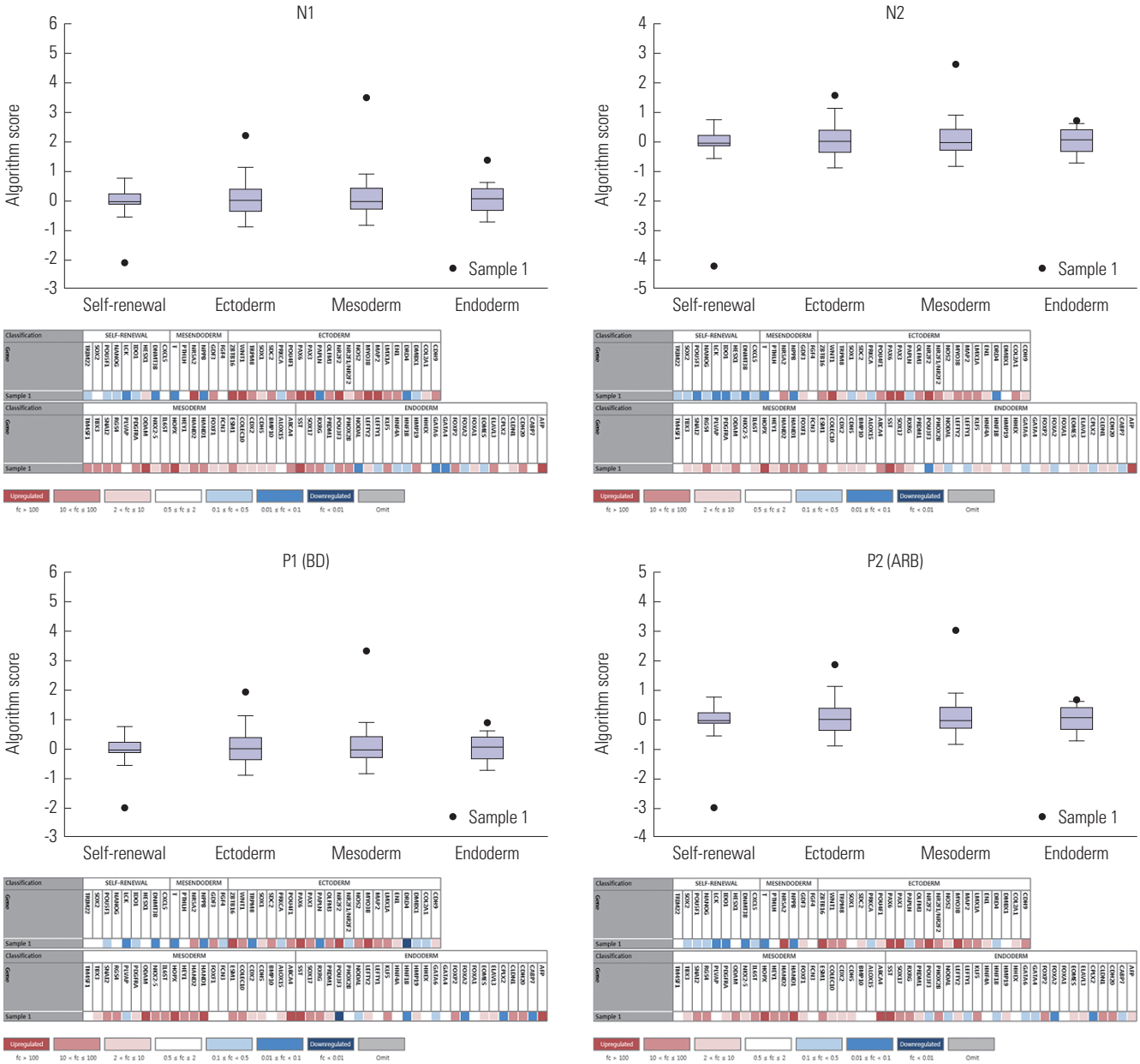

Fig. 5. Teratoma analyses of iPSC lines. Teratoma studies from normal controls and patients demonstrated derivatives from the endodermal, ectodermal, and mesodermal germ lineages. iPSC, induced pluripotent stem cell.

https://doi.org/10.3349/ymj.2020.61.9.816

markers including c-MYC, OCT4, SOX2, NANOG, and KLF4 (Fig. 4), and teratoma studies confirmed that 7-day embryoid bodies derived from iPSC showed markers for all three lineages (Fig. 5).

Differentiation of iPSC into RPE cell

Light microscopy and RT-PCR were performed to confirm the differentiation of iPSC into the RPE cell. RPE differentiation was performed in retinal differentiation media until approximately Day 40–90, at which characteristic polygonality and pigmentation of the RPE could be confirmed on light microscopy (Fig. 6A). RT-PCR revealed the expressions of a characteristic RPE gene *BEST1* and a tight junction gene OCCLUDIN (Fig. 6B).

Cytological and functional analysis of ARB iPSC-RPE

Morphological characteristics of the RPE were evaluated using confocal microscopy and immunocytochemistry. The rate of fluid flow across iPSC-RPE monolayer on transwell insert was measured to compare apical to basal fluid transports by the RPE. Immunocytochemistry revealed uniform tight junction protein ZO-1 in both ARB and control iPSC-RPE (Fig. 7). There was no significant difference in TER measurements between ARB patient, autosomal dominant BD patient, and normal control (Table 2). TER measurements obtained from ARB iPSC-RPE

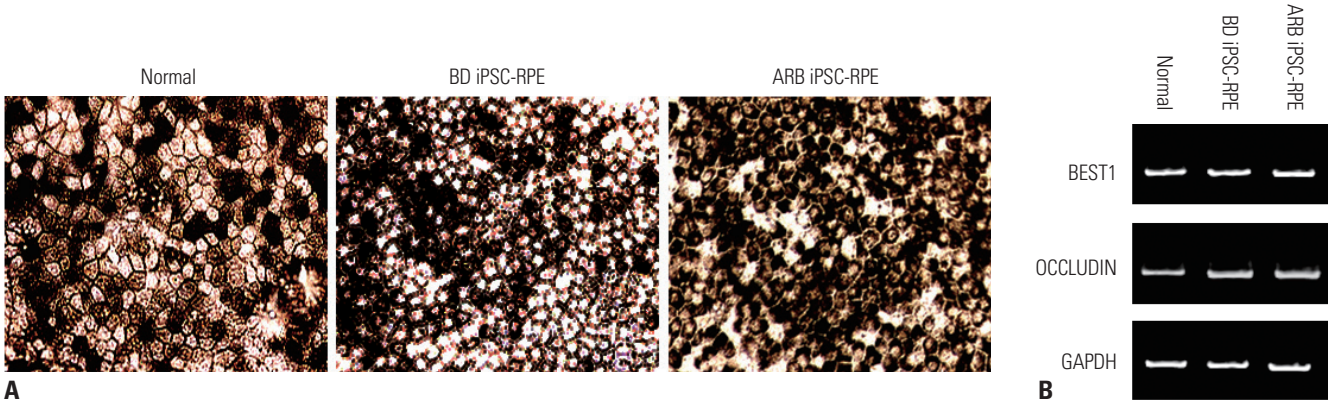

Fig. 6. Differentiation of induced pluripotent stem cells into functional RPE cells. (A) Characteristic polygonality and pigmentation of the RPE could be confirmed using light microscopy. (B) RT-PCR revealed the expressions of a characteristic RPE gene BEST1 and a tight junction gene OCCLUDIN. GAPDH was as a loading control. BD iPSC-RPE, Best disease induced pluripotent stem cell retinal pigment epithelium; ARB iPSC-RPE, autosomal recessive bestrophinopathy induced pluripotent stem cell retinal pigment epithelium.

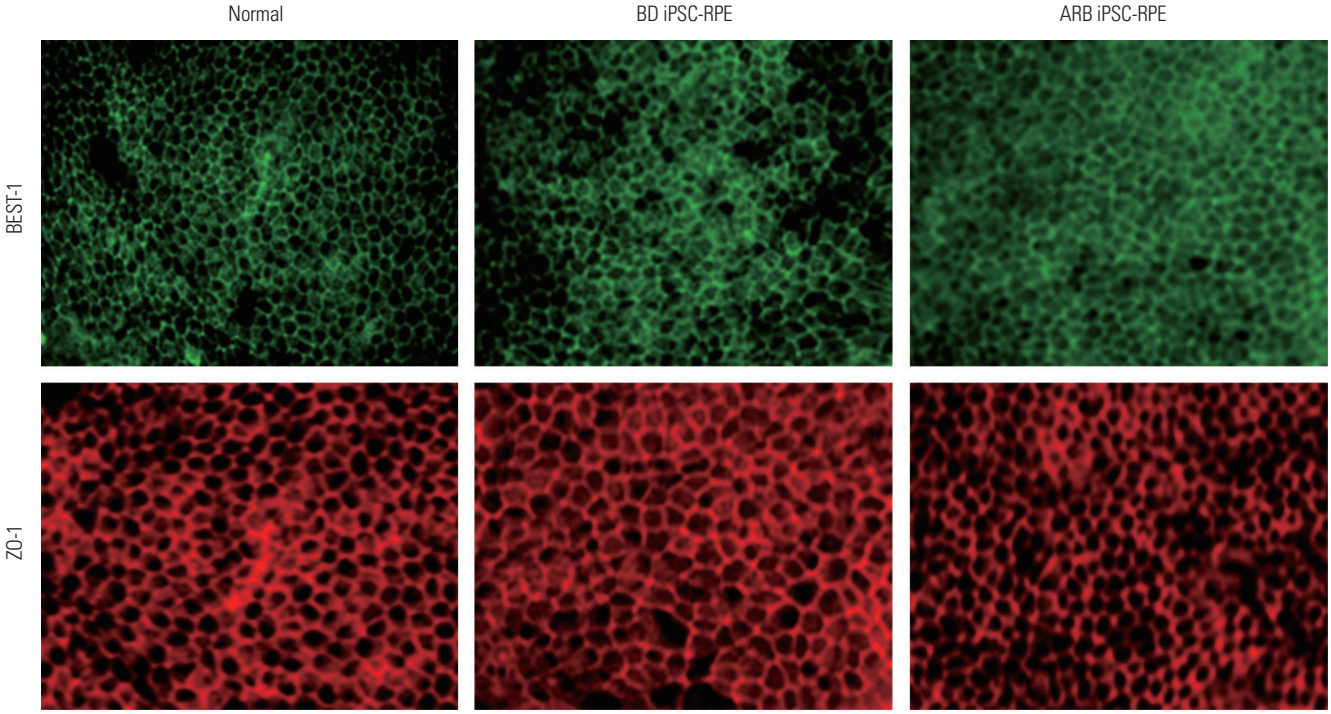

Fig. 7. Immunocytochemistry in iPSC-RPE. Immunocytochemistry for BEST1 and ZO-1 showed uniform morphology and tight junction in Best disease, ARB, and control iPSC-RPE. BD iPSC-RPE, Best disease induced pluripotent stem cell retinal pigment epithelium; ARB iPSC-RPE, autosomal recessive bestrophinopathy induced pluripotent stem cell retinal pigment epithelium.

(290.00±10.24 Ω) were similar to those of BD iPSC-RPE (312.67±23.84 Ω, p=0.936) and control iPSC-RPE (305.83±13.33 Ω, p=0.335) (Fig. 8A). The rate of fluid flow was the lowest in ARB iPSC-RPE (0.12±0.01), and was significantly lower than those of control iPSC-RPE (0.35±0.02, p<0.001) and BD iPSC-RPE (0.29±0.02, p<0.001) (Fig. 8B).

Gene expression profiles of ARB iPSC-RPE

RNA-sequencing was performed to identify the differences in gene expression profiles between ARB iPSC-RPE, BD iPSC-RPE, and control iPSC-RPE. Gene Set Enrichment Analysis showed that ARB iPSC-RPE exhibited significant enrichment of epithelial-mesenchymal transition (EMT) gene set compared with control iPSC-RPE (Fig. 9A). Genes encoding TNF-α signaling via NF-κB were also significantly enriched in ARB iPSC-RPE compared with control iPSC-RPE (Fig. 9B). ARB iPSC-RPE showed similar results compared with BD iPSC-RPE (Fig. 9C and D).

DISCUSSION

In this study, a human iPSC model of ARB was evaluated to understand its pathophysiology, which revealed a functional deficiency rather than anatomical defects. Morphological characteristics, gene expression, and epithelial integrity of ARB iPSC were comparable to those of normal control. Fluid transport from apical to basal was more reduced in ARB iPSC-RPE than in autosomal dominant BD iPSC-RPE.

RPE-based disorders appear to be ideal for human iPSC modeling, given the ease and extent to which this cell type can be generated, manipulated, and tested. The maturation state of iPSC-RPE can be also monitored in live cultures using morphological features and measurement of TER.[24] Singh, et al.[16] developed a iPSC-RPE model of Best vitelliform macular dystrophy utilizing these characteristics of human RPE. They demonstrated that RPE from mutant iPSC displayed disrupted fluid flux and increased accrual of autofluorescent material after long-term photoreceptor outer segment feeding. Therefore, human iPSC-derived RPE is a potentially useful tool for disease modeling and therapeutics in human retinal degenerative diseases.

Defect in transcellular fluid in iPSC-RPE was more prominent in ARB patient than in autosomal dominant BD patient, which could explain the common macular edema and subretinal fluid in ARB patient. The macular pathology in BD patients usually seems to be stable until the late stage of the disease course, and most patients retain moderate visual acuity until later in life.[25,26] Therefore, the result may also suggest that BD is caused by the cumulative effects of one or more subtle alterations in RPE physiology. Other cytological examinations, including morphological characteristics, gene expression, and epithelial integrity, revealed similar results between ARB iPSC-RPE and normal control. Considering the more prominent defect in transcellular fluid in ARB iPSC-RPE than in autosomal dominant BD iPSC-RPE, these findings may suggest that ARB is caused by *BEST1* dysfunction.

EMT is a biologic process resulting in the conversion of epithelial cells to myofibroblasts.[27,28] It is characterized by the loss of epithelial characteristics, which includes apical-basolateral polarity and cell-cell adhesions.[29] Increased expressions of transforming growth factor-β, α-smooth muscle actin, extracellular

Table 2. TER Measurement and the Rate of Fluid Flow in BD iPSC-RPE and ARB iPSC-RPE

	Control	BD iPSC-RPE	*p* value	ARB iPSC-RPE	*p* value
TER (Ω*cm^2)	305.83±13.33	312.67±23.84	0.936	290.00±10.24	0.335
Fluid flow (μL/hr/cm^2)	0.35±0.02	0.29±0.02	0.038	0.12±0.01	<0.001

ARB iPSC-RPE, autosomal recessive bestrophinopathy induced pluripotent stem cell retinal pigment epithelium, BD iPSC-RPE, Best disease induced pluripotent stem cell retinal pigment epithelium, TER, transepithelial resistance

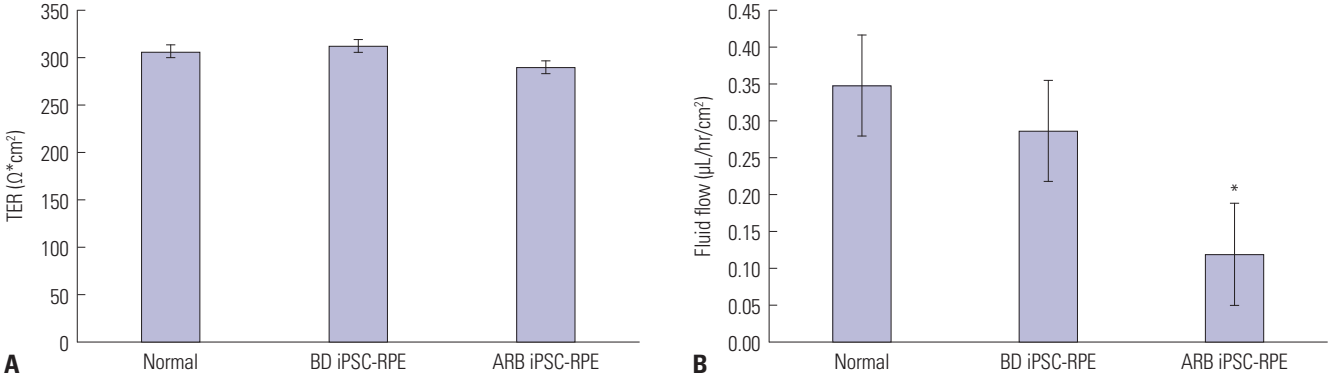

Fig. 8. TER measurements and the quantification of fluid movement in BD iPSC-RPE, ARB iPSC-RPE, and control iPSC-RPE. (A) TER were comparable between patients and control iPSC-RPE. (B) The rate of fluid flow was the lowest in ARB iPSC-RPE, and was significantly lower than those of control iPSC-RPE and BD iPSC-RPE. *p<0.001 compared with control or BD iPSC-RPE. BD iPSC-RPE, Best disease induced pluripotent stem cell retinal pigment epithelium; ARB iPSC-RPE, autosomal recessive bestrophinopathy induced pluripotent stem cell retinal pigment epithelium; TER: transepithelial resistance.

https://doi.org/10.3349/ymj.2020.61.9.816

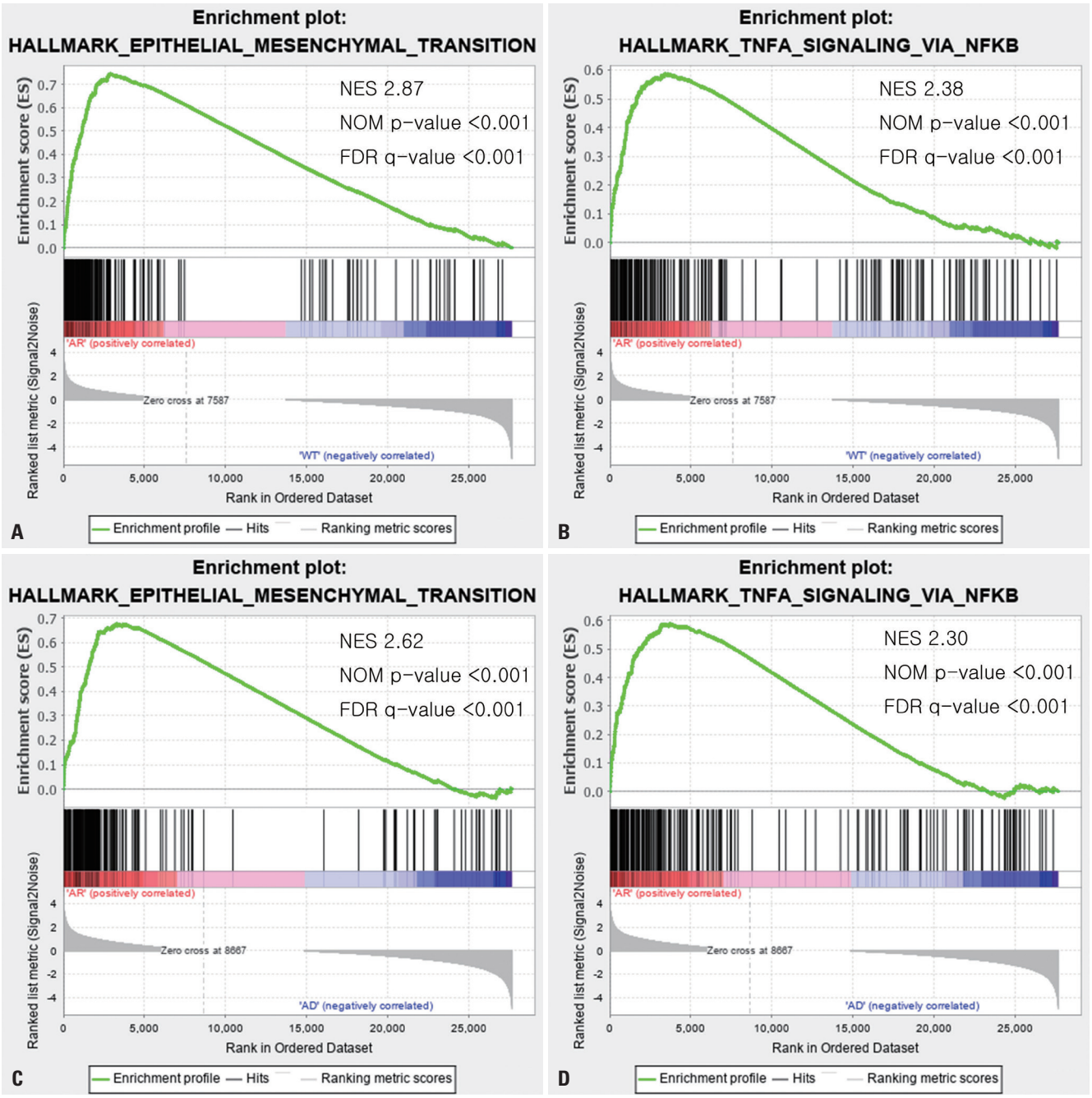

Fig. 9. GSEA plots showed that epithelial-mesenchymal transition gene set and TNF-α signaling via NF-κB gene set were significantly enriched in ARB iPSC-RPE compared with control iPSC-RPE (A and B) or BD iPSC-RPE (C and D). GSEA, Gene Set Enrichment Analysis; ARB iPSC-RPE, autosomal recessive bestrophinopathy induced pluripotent stem cell retinal pigment epithelium; BD iPSC-RPE, Best disease induced pluripotent stem cell retinal pigment epithelium; FDR, false discovery rate; NES, normalized enrichment score; NOM, nominal.

matrix proteins collagen type 1, and matrix metalloproteinases induce this process.[27,29-31] EMT of the RPE is known to be related to the pathogenesis of subretinal fibrosis in various retinal diseases, including age-related macular degeneration.[32-34] NF-κB activation by TNF-α is well-known to play a crucial role in EMT.[35-38] Recently, an association between EMT genes and genes involved in NF-κB activation has been reported.[37,39,40] Gene expression profiles of ARB iPSC-RPE exhibited significant enrichment of EMT gene set compared to control iPSC-RPE or BD iPSC-RPE. Genes encoding TNF-α signaling via NF-κB was also enriched in ARB iPSC-RPE compared to control iPSC-RPE or BD iPSC-RPE. These results indicate that inhibiting EMT and NF-κB activation in the RPE could be a potential therapeutic target for ARB.

The lack of peripheral retinal findings in BD and ARB is possibly related to the capacity for RPE cells to withstand the pres-

ence of dysfunctional *BEST1*. This difference in phenotype between central and peripheral retina in BD and ARB could be explained by regional differences in the RPE or superimposed environmental stress upon the macular RPE.[16] Further studies are necessary to evaluate whether iPSC-RPE cells are more similar to macula or peripheral retina. Studies on ADVIRC iPSC-RPE would be also useful in finding the difference between central and peripheral lesions of bestrophinopathy.

In conclusion, this study established an in vitro model of ARB, which showed a functional deficiency rather than anatomical defects. Fluid transport from apical to basal was significantly reduced in ARB iPSC-RPE compared to that of autosomal dominant BD iPSC-RPE. ARB may be caused by RPE dysfunction following *BEST1* mutation.

ACKNOWLEDGEMENTS

This research was supported by the Basic Science Research Program through the National Research Foundation of Korea (NRF) under 2016R1D1A1A02937349 and by a faculty research grant of Yonsei University College of Medicine (6-2017-0069). The funding organizations had no role in the design or conduct of this research.

AUTHOR CONTRIBUTIONS

Conceptualization: Ji Hwan Lee and Christopher Seungkyu Lee. Data curation: Ji Hwan Lee and Jin-ok Oh. Formal analysis: Ji Hwan Lee. Investigation: all authors. Methodology: all authors. Project administration: Christopher Seungkyu Lee. Resources: all authors. Software: Ji Hwan Lee and Jin-ok Oh. Supervision: all authors. Validation: all authors. Visualization: Ji Hwan Lee and Jin-ok Oh. Writing-original draft: Ji Hwan Lee. Writing-review & editing: all authors. Approval of final manuscript: all authors.

ORCID iDs

Ji Hwan Lee https://orcid.org/0000-0003-1759-8195
Jin-ok Oh https://orcid.org/0000-0002-1997-1670
Christopher Seungkyu Lee https://orcid.org/0000-0001-5054-9470

REFERENCES

1. Forsman K, Graff C, Nordström S, Johansson K, Westermark E, Lundgren E, et al. The gene for Best's macular dystrophy is located at 11q13 in a Swedish family. Clin Genet 1992;42:156-9.
2. Stone EM, Nichols BE, Streb LM, Kimura AE, Sheffield VC. Genetic linkage of vitelliform macular degeneration (Best's disease) to chromosome 11q13. Nat Genet 1992;1:246-50.
3. Marmorstein AD, Marmorstein LY, Rayborn M, Wang X, Hollyfield JG, Petrukhin K. Bestrophin, the product of the Best vitelliform macular dystrophy gene (VMD2), localizes to the basolateral plasma membrane of the retinal pigment epithelium. Proc Natl Acad Sci U S A 2000;97:12758-63.
4. O'Gorman S, Flaherty WA, Fishman GA, Berson EL. Histopathologic findings in Best's vitelliform macular dystrophy. Arch Ophthalmol 1988;106:1261-8.
5. Guziewicz KE, Sinha D, Gómez NM, Zorych K, Dutrow EV, Dhingra A, et al. Bestrophinopathy: an RPE-photoreceptor interface disease. Prog Retin Eye Res 2017;58:70-88.
6. Boon CJF, Klevering BJ, Leroy BP, Hoyng CB, Keunen JEE, den Hollander AI. The spectrum of ocular phenotypes caused by mutations in the BEST1 gene. Prog Retin Eye Res 2009;28:187-205.
7. Best F. II. Über eine hereditäre Maculaaffektion. Ophthalmologica 1905;13:199-212.
8. Renner AB, Tillack H, Kraus H, Krämer F, Mohr N, Weber BHF, et al. Late onset is common in best macular dystrophy associated with VMD2 gene mutations. Ophthalmology 2005;112:586-92.
9. Deutman AF. Electro-oculography in families with vitelliform dystrophy of the fovea. Detection of the carrier state. Arch Ophthalmol 1969;81:305-16.
10. Meunier I, Sénéchal A, Dhaenens CM, Arndt C, Puech B, Defoort-Dhellemmes S, et al. Systematic screening of BEST1 and PRPH2 in juvenile and adult vitelliform macular dystrophies: a rationale for molecular analysis. Ophthalmology 2011;118:1130-6.
11. Burgess R, Millar ID, Leroy BP, Urquhart JE, Fearon IM, De Baere E, et al. Biallelic mutation of BEST1 causes a distinct retinopathy in humans. Am J Hum Genet 2008;82:19-31.
12. Gerth C, Zawadzki RJ, Werner JS, Héon E. Detailed analysis of retinal function and morphology in a patient with autosomal recessive bestrophinopathy (ARB). Doc Ophthalmol 2009;118:239-46.
13. Wittström E, Ekvall S, Schatz P, Bondeson ML, Ponjavic V, Andréasson S. Morphological and functional changes in multifocal vitelliform retinopathy and biallelic mutations in BEST1. Ophthalmic Genet 2011;32:83-96.
14. Zhao L, Grob S, Corey R, Krupa M, Luo J, Du H, et al. A novel compound heterozygous mutation in the BEST1 gene causes autosomal recessive Best vitelliform macular dystrophy. Eye (Lond) 2012;26:866-71.
15. Luo J, Lin M, Guo X, Xiao X, Li J, Hu H, et al. Novel BEST1 mutations and special clinical characteristics of autosomal recessive bestrophinopathy in Chinese patients. Acta Ophthalmol 2019;97:247-59.
16. Singh R, Shen W, Kuai D, Martin JM, Guo X, Smith MA, et al. iPS cell modeling of Best disease: insights into the pathophysiology of an inherited macular degeneration. Hum Mol Genet 2013;22:593-607.
17. Meyer JS, Shearer RL, Capowski EE, Wright LS, Wallace KA, McMillan EL, et al. Modeling early retinal development with human embryonic and induced pluripotent stem cells. Proc Natl Acad Sci U S A 2009;106:16698-703.
18. Meyer JS, Howden SE, Wallace KA, Verhoeven AD, Wright LS, Capowski EE, et al. Optic vesicle-like structures derived from human pluripotent stem cells facilitate a customized approach to retinal disease treatment. Stem Cells 2011;29:1206-18.
19. Phillips MJ, Wallace KA, Dickerson SJ, Miller MJ, Verhoeven AD, Martin JM, et al. Blood-derived human iPS cells generate optic vesicle-like structures with the capacity to form retinal laminae and develop synapses. Invest Ophthalmol Vis Sci 2012;53:2007-19.
20. Stamer WD, Bok D, Hu J, Jaffe GJ, McKay BS. Aquaporin-1 channels in human retinal pigment epithelium: role in transepithelial water movement. Invest Ophthalmol Vis Sci 2003;44:2803-8.
21. Bolger AM, Lohse M, Usadel B. Trimmomatic: a flexible trimmer for Illumina sequence data. Bioinformatics 2014;30:2114-20.
22. Kim D, Paggi JM, Park C, Bennett C, Salzberg SL. Graph-based genome alignment and genotyping with HISAT2 and HISAT-genotype. Nat Biotechnol 2019;37:907-15.
23. Subramanian A, Tamayo P, Mootha VK, Mukherjee S, Ebert BL, Gillette MA, et al. Gene set enrichment analysis: a knowledge-based approach for interpreting genome-wide expression profiles. Proc

Natl Acad Sci U S A 2005;102:15545-50.
24. Gamm DM, Phillips MJ, Singh R. Modeling retinal degenerative diseases with human iPS-derived cells: current status and future implications. Expert Rev Ophthalmol 2013;8:213-6.
25. Fishman GA, Baca W, Alexander KR, Derlacki DJ, Glenn AM, Viana M. Visual acuity in patients with best vitelliform macular dystrophy. Ophthalmology 1993;100:1665-70.
26. Ponjavic V, Eksandh L, Andréasson S, Sjöström K, Bakall B, Ingvast S, et al. Clinical expression of Best's vitelliform macular dystrophy in Swedish families with mutations in the bestrophin gene. Ophthalmic Genet 1999;20:251-7.
27. Kalluri R, Neilson EG. Epithelial-mesenchymal transition and its implications for fibrosis. J Clin Invest 2003;112:1776-84.
28. Kobayashi M, Tokuda K, Kobayashi Y, Yamashiro C, Uchi SH, Hatano M, et al. Suppression of epithelial-mesenchymal transition in retinal pigment epithelial cells by an MRTF-A inhibitor. Invest Ophthalmol Vis Sci 2019;60:528-37.
29. Mamuya FA, Duncan MK. aV integrins and TGF-β-induced EMT: a circle of regulation. J Cell Mol Med 2012;16:445-55.
30. Tan TK, Zheng G, Hsu TT, Wang Y, Lee VWS, Tian X, et al. Macrophage matrix metalloproteinase-9 mediates epithelial-mesenchymal transition in vitro in murine renal tubular cells. Am J Pathol 2010;176:1256-70.
31. Moustakas A, Heldin P. TGFβ and matrix-regulated epithelial to mesenchymal transition. Biochim Biophys Acta 2014;1840:2621-34.
32. Friedlander M. Fibrosis and diseases of the eye. J Clin Invest 2007;117:576-86.
33. Tamiya S, Kaplan HJ. Role of epithelial-mesenchymal transition in proliferative vitreoretinopathy. Exp Eye Res 2016;142:26-31.
34. Ishikawa K, Kannan R, Hinton DR. Molecular mechanisms of subretinal fibrosis in age-related macular degeneration. Exp Eye Res 2016;142:19-25.
35. Bates RC, Mercurio AM. Tumor necrosis factor-alpha stimulates the epithelial-to-mesenchymal transition of human colonic organoids. Mol Biol Cell 2003;14:1790-800.
36. Huber MA, Azoitei N, Baumann B, Grünert S, Sommer A, Pehamberger H, et al. NF-kappaB is essential for epithelial-mesenchymal transition and metastasis in a model of breast cancer progression. J Clin Invest 2004;114:569-81.
37. Maier HJ, Schmidt-Strassburger U, Huber MA, Wiedemann EM, Beug H, Wirth T. NF-kappaB promotes epithelial-mesenchymal transition, migration and invasion of pancreatic carcinoma cells. Cancer Lett 2010;295:214-28.
38. Li CW, Xia W, Huo L, Lim SO, Wu Y, Hsu JL, et al. Epithelial-mesenchymal transition induced by TNF-α requires NF-κB-mediated transcriptional upregulation of Twist1. Cancer Res 2012;72:1290-300.
39. Chung CH, Parker JS, Ely K, Carter J, Yi Y, Murphy BA, et al. Gene expression profiles identify epithelial-to-mesenchymal transition and activation of nuclear factor-kappaB signaling as characteristics of a high-risk head and neck squamous cell carcinoma. Cancer Res 2006;66:8210-8.
40. Pires BRB, Mencalha AL, Ferreira GM, de Souza WF, Morgado-Díaz JA, Maia AM, et al. NF-kappaB is involved in the regulation of EMT genes in breast cancer cells. PLoS One 2017;12:e0169622.